The Baroclinic Instability Process: from linear to non-linear regime

Tiago Carrilho Biló
C# 11950866
tcb46@miami.edu

Rosenstiel School of Marine and Atmospheric Science - Geophysical Fluid Dynamics II (MPO 711) - Project Report

April 28, 2016

1 Introduction

The ability of describing stability properties of currents is intimately related to our capacity of predicting the variability of the large-scale atmospheric and oceanic circulation. Therefore if we understand how perturbations grow and modify currents, we can predict a wide-range of important natural phenomena (e. g., *Vallis*, 2006). The development and propagation of mesoscale ocean eddies are governed by complicated non-linear dynamics. However the initial stages of eddy formation are related to growing wave-like perturbations (or meander) that can be predicted by the linear instability theory (*Pedlosky*, 1987).

The present report is part of the **Geophysical Fluid Dynamics (MPO 711)** coursework project. Here I described a numerical experiment that predicts the development of perturbations in a 2-layer flow. The goal is to identify and describe the periods that the linear instability theory could be applied, and how perturbations develop in a idealized ocean.

2 Model Setup Overview

The numerical experiment was performed using a model that integrates the full potential vorticity (PV) equation for a 2-layer zonal channel system under the Quasi-Geostrophic (QG) approximation. Assuming the coordinates system components being: time (t), along channel (x), and cross-channel (y), the PV-

equation will be

$$\begin{cases} Q_i = \bar{q}_i + q_i, \\ \frac{DQ_i}{Dt} = \frac{\partial \bar{q}_i}{\partial t} + \frac{\partial q_i}{\partial t} + J(\bar{\psi}_i, \bar{q}_i) + J(\bar{\psi}_i, q_i) + J(\psi_i, \bar{q}_i) + J(\psi_i, q_i) + \mathbb{F} = 0, \end{cases} \tag{1}$$

where the index i corresponds to the respective layer of the ocean (i. e., $i = 1$ is the upper layer and $i = 2$ the lower layer), ψ is the stream function, Q is the PV, $\mathbb{F}$ the friction terms (i. e., lateral and bottom friction), and $J(a,b) = \frac{\partial a}{\partial x}\frac{\partial b}{\partial y} - \frac{\partial a}{\partial y}\frac{\partial b}{\partial x}$ is the Jacobian operator. The over bars denote the mean zonal background flow ψ_i and q_i.

The channel was set to have constant depth, therefore Q_i is given by

$$\begin{cases} Q_1 = \nabla^2 \Psi_1 + \beta_0 y - \frac{1}{R_1}(\Psi_1 - \Psi 2), \\ Q_2 = \nabla^2 \Psi_2 + \beta_0 y - \frac{1}{R_2}(\Psi_2 - \Psi 1), \end{cases} \tag{2}$$

where ∇^2 is the horizontal Laplacian operator, β_0 is the meridional change rate of the planetary vorticity, and $R_i = \frac{g'}{f_0^2} H_i$[1][2][3]. From Equation 3, we can isolate the PV perturbations q_i as

$$\begin{cases} q_1 = \nabla^2 \psi_1 - \frac{1}{R_1}(\psi_1 - \psi_2), \\ q_2 = \nabla^2 \psi_2 - \frac{1}{R_2}(\psi_2 - \psi_1). \end{cases} \tag{3}$$

All the model parameters are listed in Table 1.

Table 1: Necessary model parameters: mean velocity field (U_i), layer thickness (H_i), channel width (L), reduced gravity (g'), Coriolis parameter (f_0), meridional change rate of the planetary vorticity (β_0), and the friction terms.

U_1 (m s^{-1})	0.06	U_2 (m s^{-1})	0.0
H_1 (m)	1000	H_2 (m)	3000
L (km)	1800	g' (m s^{-2})	5.75×10^{-3}
f_0 (s^{-1})	8.3×10^{-5}	β_0 (m^{-1} s^{-1})	2×10^{-11}
Lateral Laplacian viscosity (m^2 s^{-1})	50	Bottom friction coeff. (s^{-1})	10^{-7}

[1] g' =reduced gravity term;
[2] H_i =layer thickness;
[3] f_0 =Coriolis parameter.

3 Results and Discussion

3.1 Outputs Overview

The model integrates Equation 1 with a time step of 18 min for 1200 days. Every 10 days, the perturbations stream function (ψ_i), eddy kinetic energy (EKE) at each layer and eddy potential energy (EPE) were saved[4]. Figures 1 and 2 depict the snapshots of ψ_1 and ψ_2, respectively. Note that in both layers, the perturbations grow with time and have similar spatial structures, however the amplitudes in the shallower upper layer are higher (colorbars where adjusted to emphasize the gradients).

Another interesting characteristic is related to the radical change in the perturbations structure between day 150 and 250. In the first 150 days, the perturbations have a wave-like structure that grows in time and propagates along the channel. Then the amplitudes become significantly higher, it stops growing after day 550, the wave-like pattern breaks down and a pattern of zonal meandering currents and counter-currents dominates the fields.

This regime change is associated with the non-linear term in Equation 1 [i. e., $J(\psi_i, q_i)$]. When the model starts, the perturbations amplitudes are small so the linear terms dominates the dynamics. In this initial stage, the perturbations grow due to linear instability processes. Since the background state does not have horizontal velocity shear (only vertical shear, $U_1 \neq U_2$), linear baroclinic instability drains available potential energy from the mean flow and transfers it to the perturbations. Therefore the wave-like pattern seen in the first 150 days is the "signature" of the most linear unstable vorticity wave [or mode] (*Pedlosky*, 1987).

In order to take a better look at the regime transition, I plotted the ψ_1 fields snapshots from day 150, 170, 190, 210, 230 and 250 in Figure 3. Note the wave starts "breaking" between day 170 and 200 at $y =$300 km and 1500 km. After day 230, eddies start forming in the domain's interior and edges revealing a complete non-linear regime. Although the model used in the present study is idealized and simple, this kind of behavior are present in the real ocean. Linear instability processes are responsible for triggering meandering formation of major currents and for its variability [e. g., Gulf Stream, Kuroshio, Brazil Current, etc] (e. g., *Johns*, 1988; *James*, 1996; *Silveira et al.*, 2008).

[4]The term (eddy energy) refers to the energy in the perturbations fields (or eddy field).

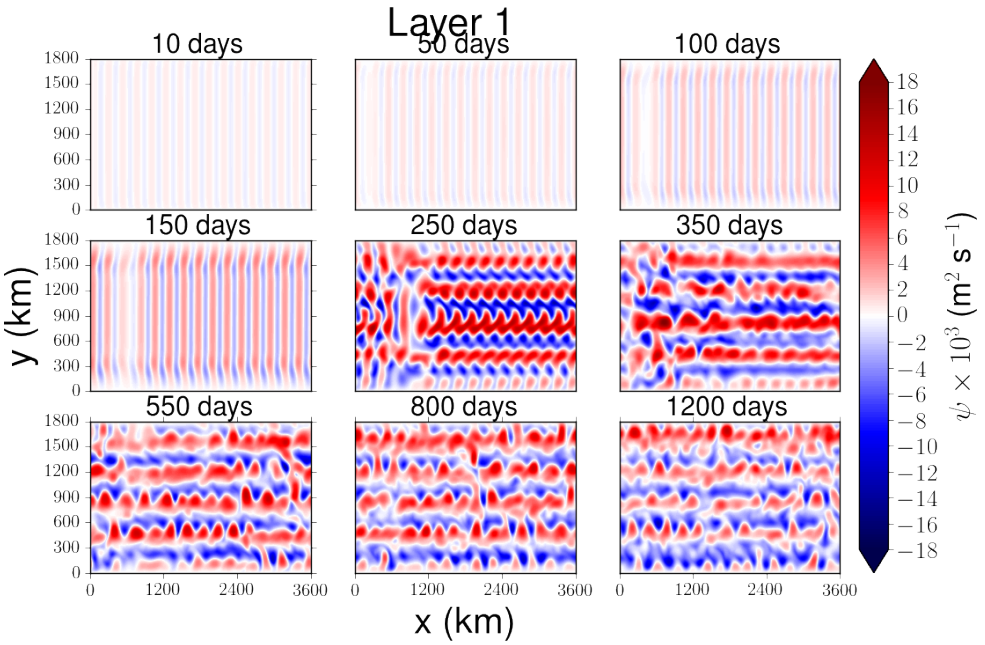

Figure 1: Perturbations stream function fields in the upper layer (i. e., Layer 1).

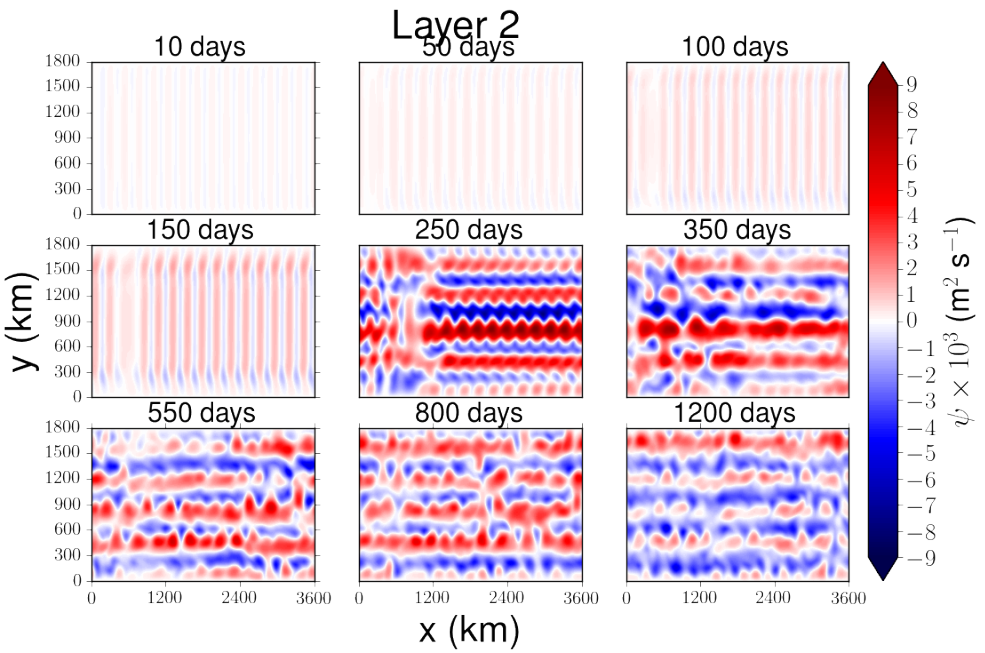

Figure 2: Perturbations stream function fields in the lower layer (i. e., Layer 2).

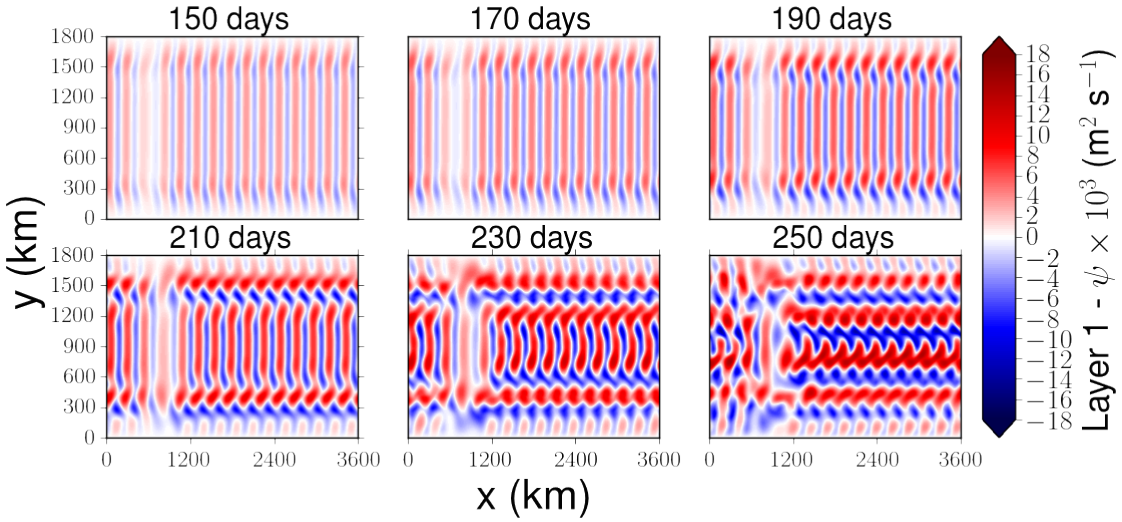

Figure 3: Perturbations stream function fields in the upper layer (i. e., Layer 1) at day 150, 170, 190, 210, 230 and 250.

We also can verify some of the described mechanisms by looking at the eddy energies evolution with time (Figure 4). As expected, the system has a stage where the energy in the eddy field grows exponentially ($t \leq$250 days) then the waves break in eddies which looses energy to the mean state. Note that most of exponential growth period is within the linear dynamics regime, corroborating the idea of exponential growth driven by linear instability.

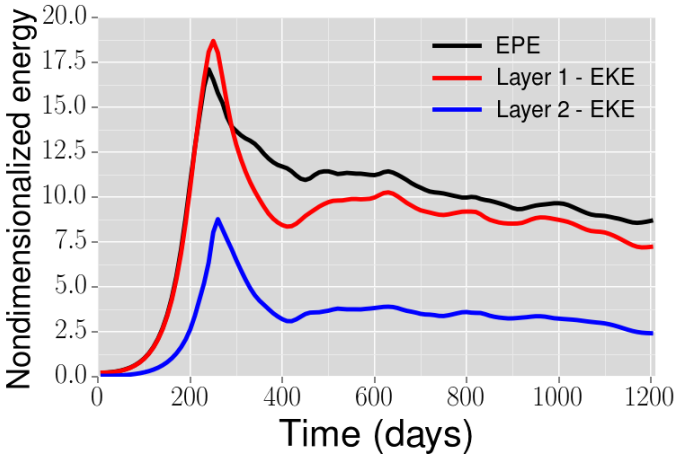

Figure 4: Evolution of the eddy potential energy (EPE) of the system, an the eddy kinetic energy (EKE) in the different layers.

3.2 Linear Regime

As mentioned before, the linear regime is characterized by perturbations of small amplitudes yielding a $J(\psi_i, q_i)$ negligible when compared to the linear terms. In order to exemplify how large $J(\psi_i, q_i)$ can get, I computed the non-linear Jacobian term and plot its evolution in Figure 5. As expected the non-linear terms becomes more significant after 190 days, changing the regime. Moreover, the maximum values of $J(\psi_i, q_i)$ were found at approximately day 250 (not shown) which represents the peak in the EKE (Figure 4).

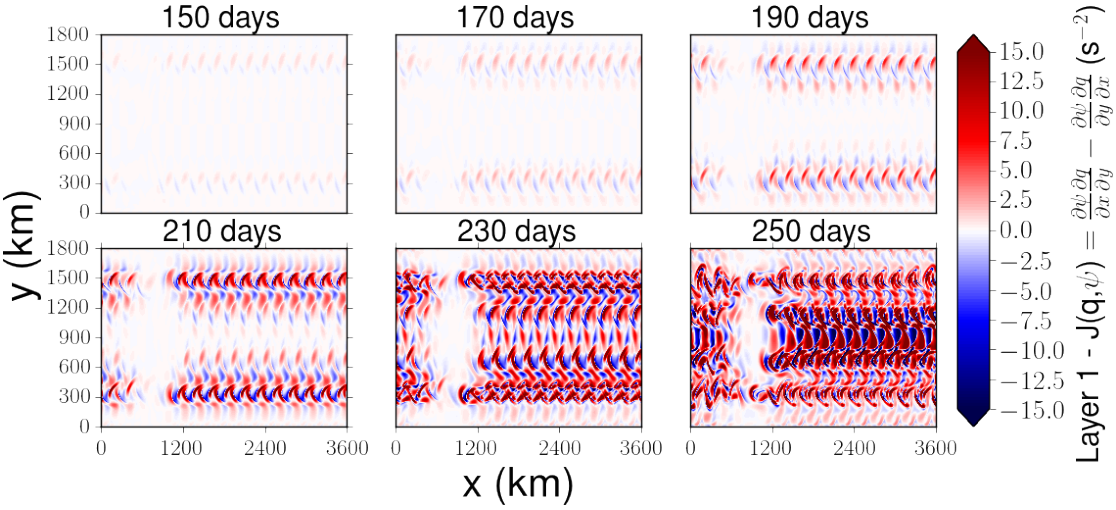

Figure 5: Evolution of the non-linear term $J(\psi_1, q_1)$ in the upper layer at day 150, 170, 190, 210, 230 and 250.

In the first 200 days, we can define the properties of the most unstable linear wave (i. e., wavelength, phase speed and exponential growth rate). Analytical solutions can be found for simpler systems and tested against the estimates performed in this study, which I will not do in this study. Since the linear waves propagate along the channel, I was able to characterize it by analyzing a Hovmöller diagram.

Figure 6 upper panel shows the diagram in the middle of the channel (i. e., y =900 km). The perturbations have wavelength [i. e., the distance between two consecutive crests (or troughs)] of ∼200 km. Additionally the tilting of the parallel crests (or troughs) yielded a eastward phase propagation of approximately 0.47×10^{-2} m s^{-1}.

In order to estimate its growth rate, I tracked a perturbation crest in the first 200 days (dashed black line in the Hovmöller diagram) and plotted it against time in the Figure 6 lower panel. Then, I fitted an

exponential curve to the crest amplitude in the least squares sense of the type $a \times e^{-bt} + c$, where b is the growth rate of $\sim 1.28 \times 10^{-2}$ day^{-1}.

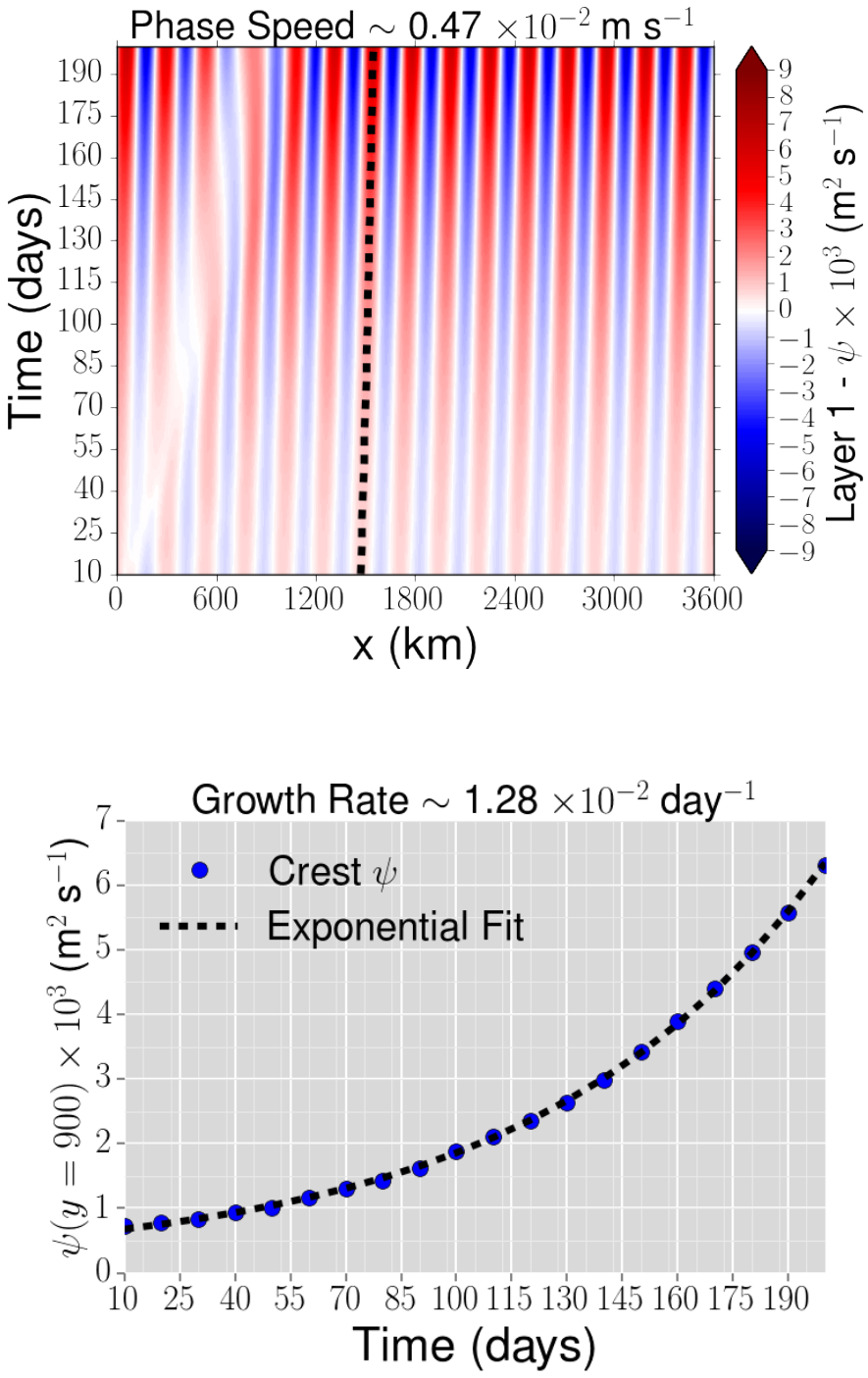

Figure 6: Hovmöller diagram of ψ_1 in the first 200 days (upper panel). The dashed line represent the crest evolution presented in the lower panel.

References

James, C. (1996), Kuroshio Instabilities in the East of China Sea - Observations, Modeling, and Comparision with the Gulf Stream, Ph.D. thesis, University of Rhode Island.

Johns, W. E. (1988), One-dimensional baroclinically unstable waves on the Gulf Stream potential vorticity gradient near Cape Hatteras, *Dynam. Atmos. Oceans*, *11*, 323–350.

Pedlosky, J. (1987), *Geophysical Fluid Dynamics*, second ed., Springer.

Silveira, I. C., J. A. M. Lima, A. C. K. Schimdt, W. Ceccopieri, A. Satori, C. P. F. Francisco, and R. F. C. Fontes (2008), Is the meander growth in the Brazil Current System off Southeast Brazil due to baroclinic instability?, *Dynam. Atmos. Oceans*, *45*, 187–207.

Vallis, G. K. (2006), *Atmospheric and Oceanic Fluid Dynamics, Fundamentals and Large-Scale Circulation*, Cambridge Universuty Press.